Serotonin receptor imaging: Parsey reviews potential clinical applications of molecular imaging of the serotonergic system and identifies challenges that remain before these can be fully implemented in routine assessment of neuropsychiatric disorders. . . . . ***Page 1495***

^{18}F-FLT and targeted therapy: De Saint-Hubert and colleagues provide a brief overview of this tracer's effectiveness in measuring proliferative changes during therapy and preview 2 articles on this topic in this issue of *JNM*. . . . ***Page 1499***

Perirectal artifact in PET/CT: Lodge and colleagues describe and detail the reasons for high-intensity regions on ^{18}F-FDG PET/CT images acquired to assess tumor involvement in the rectal area. . . . . ***Page 1501***

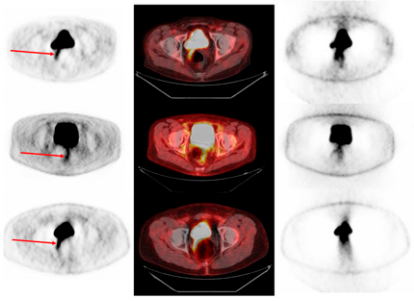

Serial PET and tumor response: Quarles van Ufford and colleagues report on a meta-analysis determining the added value of baseline ^{18}F-FDG PET in serial PET imaging to predict clinical response to systemic cytotoxic neoadjuvant treatment of solid extracerebral tumors. . . . ***Page 1507***

Automatic vs. manual contouring: Wu and colleagues compare autocontouring and manual methods for PET target definition of gross tumor volume in non–small cell lung cancer. . . . . ***Page 1517***

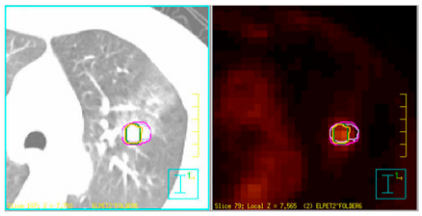

Radiolabeled peptide therapy in children: Menda and colleagues describe the results of a phase I trial of ^{90}Y-DOTATOC to determine dose–toxicity profiles in children and young adults with somatostatin receptor–positive tumors. . . . . ***Page 1524***

^{18}F-FDOPA PET in gliomas: Fueger and colleagues determine whether the degree of this tracer's uptake in brain tumors predicts tumor grade and correlates with tumor proliferative activity in patients with newly diagnosed and recurrent gliomas. . . . . ***Page 1532***

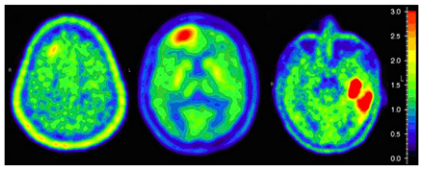

CT attenuation for CZT camera: Herzog and colleagues report on validation studies of attenuation correction using low-dose standard CT for myocardial perfusion imaging on a novel ultrafast γ-camera with cadmium-zinc-telluride detector technology. . . . . ***Page 1539***

PET/MRI and hippocampal metabolism: Cho and colleagues describe ^{18}F-FDG PET and high-resolution MR imaging of the hippocampus in healthy humans, including metabolic quantification of each hippocampal substructure. . . . ***Page 1545***

Whole-body DWI and PET: Kwee and colleagues provide an educational overview of the basic principles, clinical applications, and limitations of diffusion-weighted MRI and compare and correlate its capabilities with those of ^{18}F-FDG PET. . . . . ***Page 1549***

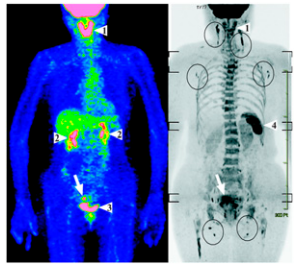

^{18}F-FLT PET of mTOR inhibition: Aide and colleagues evaluate the potential utility of ^{18}F-FLT PET in monitoring early response to treatment with mammalian target of rapamycin inhibitors using an animal model of cisplatin-resistant ovarian cancer. . . . . ***Page 1559***

IGF-1R imaging: Heskamp and colleagues describe a noninvasive, in vivo imaging method employing radiolabeled antibodies and immunoSPECT/immunoPET to visualize insulinlike growth factor 1 receptor expression in vitro and in small-animal models of breast cancer. . . . . ***Page 1565***

Inflammation and ^{99m}Tc-HDP extravasation: Lim and colleagues conduct studies in mice to explore the mechanisms underlying reported ^{99m}Tc-HDP injection site reactions in patients. . . . . ***Page 1573***

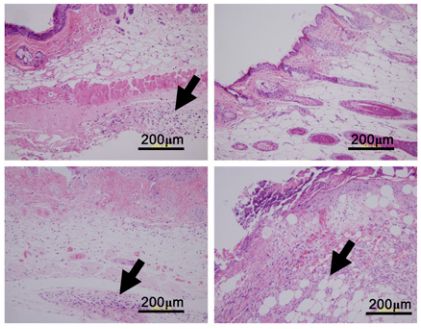

Octamouse for PET: Rominger and colleagues report on procedures for obtaining 8 simultaneous PET brain recordings from mice using an acrylic anesthesia distributor, with the dopamine $D_{2/3}$ ligand ^{18}F-fallypride serving as a test substance for brain receptor imaging. . . . . ***Page 1576***

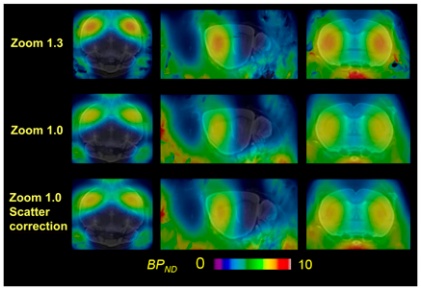

PET and phosphodiesterase: Celen and colleagues describe ^{18}F-JNJ41510417, a selective and high-affinity radioligand for in vivo PET brain imaging of phosphodiesterase-10A, and review potential applications in neuropsychiatric disorders. . . . . ***Page 1584***

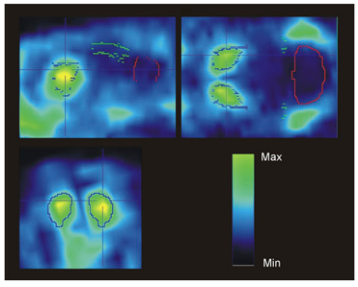

Human ^{82}Rb dosimetry: Senthamizhchelvan and colleagues reevaluate ^{82}Rb biodistribution and dosimetry in dynamic PET/CT using in vivo biokinetic measurements from healthy humans. . . . . ***Page 1592***

S values for variable voxel size: Dieudonné and colleagues present a revised voxel S values approach for dosimetry in targeted radiotherapy, allowing dose calculation for any voxel size and shape for a given SPECT or PET dataset. . . . . ***Page 1600***

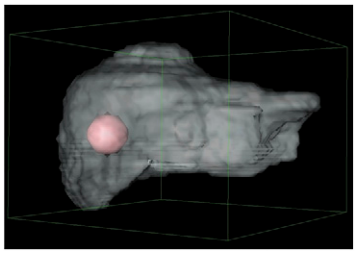

Evaluation of X-PET scanner: Prasad and colleagues evaluate the performance characteristics of the preclinical X-PET subsystem of the FLEX Triumph PET/CT scanner based on the NU 4-2008 standards of the National Electrical Manufacturers Association. . . . . ***Page 1608***

Bioimaging of α-particles: Bäck and Jacobsson describe and assess the characteristics of the α-camera, a quantitative imaging technique developed to detect α-particles in tissues ex vivo, and review potential applications in α-radioimmunotherapy. . .***Page 1616***

Rest–stress CBF with quantitative SPECT: Iida and colleagues report on multi-institutional validation of a technique that reconstructs quantitative SPECT images and assesses cerebral blood flow at rest and after acetazolamide challenge from a single SPECT session. . . . . ***Page 1624***

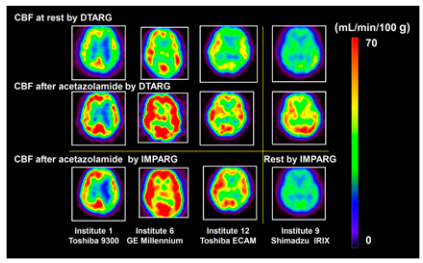

D-^{18}F-FMT in bone metastases: Zitzmann-Kolbe and colleagues detail the potential of this tracer for identifying and localizing metastatic bone lesions in a mouse model. . . . . ***Page 1632***

Imaging of macrophage trafficking: Seo and colleagues investigate the feasibility of nuclear molecular imaging using the human sodium iodide symporter hNIS as a reporter gene to monitor macrophage migration toward inflammatory foci. . . . . ***Page 1637***

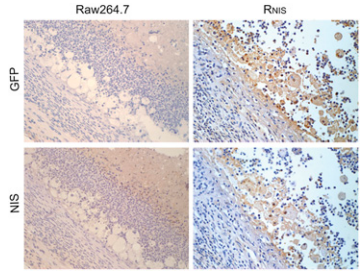

PET and renal allograft rejection: Reuter and colleagues explore the potential utility of ^{18}F-FDG PET as a method to monitor acute rejection of allogeneic renal transplants in a rat model. . . . . ***Page 1644***

ON THE COVER

The α-camera, a novel technology for the ex vivo detection of α-particles in tissues, provides rapid, quantitative imaging of α-emitting radionuclides on a near-cellular scale. The high-intensity areas in the α-camera image shown here correspond to stroma surrounding tumor cells, as seen on the histologic section. The promising characteristics of the α-camera suggest that it can assist in the development of targeted radiotherapy approaches.

See page 1620.